Chinese Journal of
POLYMER SCIENCE

RESEARCH ARTICLE

https://doi.org/10.1007/s10118-022-2723-3
Chinese J. Polym. Sci. **2022**, *40*, 1201–1212

Superior Ductile and High-barrier Poly(lactic acid) Films by Constructing Oriented Nanocrystals as Efficient Reinforcement of Chain Entanglement Network and Promising Barrier Wall

Lin Zhou, Ping-Ping Xu, Shi-Hao Ni, Ling Xu, Hao Lin, Gan-Ji Zhong*, Hua-Dong Huang*, and Zhong-Ming Li

College of Polymer Science and Engineering, State Key Laboratory of Polymer Materials Engineering, Sichuan University, Chengdu 610065, China

Electronic Supplementary Information

Abstract It is a daunting task to develop a promising strategy at an industrial scale for simultaneously ameliorating ductility and gas barrier performance of poly(lactic acid) (PLA) films in the application of green packaging. In this work, biaxial stretching and constrained annealing were employed to prepare transparent PLA films with superior ductility and barrier properties. The oriented nano-sized crystals induced by biaxial stretching were developed into regular *α* form during constrained annealing, which could not only serve as "nano-barrier wall" to impede the diffusion and dissolution of gas molecules, but also strengthen amorphous chain entanglement network as physical crosslink to enhance ductility. As a result, the as-prepared PLA films exhibited an outstanding comprehensive performance with a low oxygen and water vapor permeability coefficient of 0.733×10^{-14} $cm^3\cdot cm\cdot cm^{-2}\cdot s^{-1}\cdot Pa^{-1}$ and 3.82×10^{-14} $g\cdot cm\cdot cm^{-2}\cdot s^{-1}\cdot Pa^{-1}$, respectively, outstanding ductility with elongation at break of 66.0%, high yield strength of 84.2 MPa, and good transparency of more than 80% at 550 nm. The new insight in the relationship between microscopic amorphous and crystalline structure and macroscopic performance is conducive to alleviating the intrinsic defects of brittle and insufficient barrier PLA films without the aid of any heterogenous modifiers, facilitating their widespread commercialization in the booming sustainable packaging market.

Keywords Poly(lactic acid) films; Biaxial stretching; Constrained annealing; Gas barrier properties; Ductility

Citation: Zhou, L.; Xu, P. P.; Ni, S. H.; Xu, L.; Lin, H.; Zhong, G. J.; Huang, H. D.; Li, Z. M. Superior ductile and high-barrier poly(lactic acid) films by constructing oriented nanocrystals as efficient reinforcement of chain entanglement network and promising barrier wall. *Chinese J. Polym. Sci.* **2022**, *40*, 1201–1212.

INTRODUCTION

The increasingly serious environmental pollution resulting from non-biodegradable polymer waste has raised worldwide awareness regrading sustainability issue and triggered considerable researches on the development of environmentally friendly biodegradable polymer.[1,2] To this end, as the most promising alternative candidate to substitute for the petrochemical-based traditional polymer materials, poly(lactic acid) (PLA) has attracted extensive attentions, arising from its outstanding renewability and biodegradability, superior strength, and satisfactory transparency.[3–7] These excellent properties give PLA a great potential application prospect for serving as packaging material.[5,8] Unfortunately, the intrinsic brittleness and insufficient barrier properties of PLA can hardly meet the demanding requirements for various perishable commodities.[9–11] Hence, it is highly attractive to develop a feasible strategy in industrial production for enhancing the ductility and gas barrier properties of PLA simultaneously so as to facilitate the large-scale application of PLA in the packaging industry.

As a medium barrier material, oxygen barrier properties of PLA are superior to polyethylene (PE) and polypropylene (PP) but inferior to poly(ethylene terephthalate) (PET), and water vapor barrier properties are better than polyamide (PA) but worse than PP, PE and PET.[12,13] Thus, a growing body of work is focused on improving the barrier performance of PLA. The addition of inorganic nanoplatelets with intrinsic high barrier properties (*i.e.*, nanoclay, graphene and its derives) is one of the most commonly used strategy.[14–18] However, there are still some intractable problems that limit the large-scale production and application of PLA film in the packaging industry. On the one hand, it is difficult to realize the desirable homogeneous dispersion of nanoplatelets in PLA matrix, especially for large-scale industrial production under complex processing conditions. On the other hand, the addition of nanoplatelets inevitably disrupts the uniformity of PLA film, thus losing its valuable transparency.[19] Hence, it remains a long-standing issue to find a feasible method to enhance barrier

* Corresponding authors, E-mail: ganji.zhong@scu.edu.cn (G.J. Z.)
E-mail: hdhuang@scu.edu.cn (H.D.H.)

Received January 25, 2022; Accepted March 23, 2022; Published online June 22, 2022

properties of PLA at an industrial scale. Fortunately, it is well documented that polymer crystals analogous to nanoplatelets can also serve as impermeable barriers, thus improving the barrier properties of polymers without introducing heterogeneous components.[20–23] All the parameters pertaining to crystalline structure (*i.e.*, crystallinity, crystalline morphology, crystal polymorphism and geometric size) have a great effect on gas barrier properties.[14] For instance, as reported in our previous work, the oxygen permeability coefficient of PLA films with the crystallinity of 44.3% after isothermal crystallization at 135 °C for 60 min decreased by 46.9% compared with amorphous PLA.[20] The densely stacked hybrid shish-kebab crystals with well-interlocked boundaries induced by oriented fibrillar nucleating agent endowed PLA with outstanding gas barrier properties and its oxygen permeability coefficient was reduced by three orders of magnitude compared with amorphous PLA film.[21] Similarly, an extremely low oxygen permeability coefficient of 2×10^{-15} $cm^3\cdot cm\cdot cm^{-2}\cdot s^{-1}\cdot Pa^{-1}$ was achieved for PLA composite films by building the compact network of oriented PLA lamellae incorporated with *in situ* nanofibrils of poly(butylene adipate-*co*-terephthalate).[22] To sum up, tailoring crystalline morphology *via* constructing regular stacked lamellae network along the direction perpendicular to gas diffusion pathway is an effective approach to ameliorate gas barrier properties of PLA at an industrial scale.[22,24]

Both inorganic nanoplatelets and the well-designed polymer crystals can degrade the ductility of PLA inevitably due to their inherent brittleness. It is still an enduring task to improve the ductility of PLA and achieve the balance of stiffness and toughness. The typical brittleness of amorphous PLA at room temperature is usually attributed to its rapid physical aging. It has been demonstrated that stretching the amorphous PLA above T_g can retard physical aging and enhance the ductility significantly.[25,26] In our previous work, the structural evolution during uniaxial stretching and the mechanism for reinforcement and toughening were illustrated. After stretching, the elongation at break exhibited an impressive increase from 16.9% to 294.9% and it could be maintained even at −20 °C.[25] The strength and ductility along the tensile direction were improved dramatically. However, the mechanical properties perpendicular to the stretching direction were not enhanced, which limits the application of PLA films in the packaging field. The biaxial orientation is an efficient pathway to improve the mechanical properties in two directions simultaneously,[27–30] in which biaxial stretching could not only enhance the ductility of aged PLA film, but also endow it with eminent aging resistance.[30] In addition, many research groups have made effort to illustrate the structural evolution and the mechanism for reinforcement and toughening.[29,31–35] Unfortunately, the thermal stretching induced ductility at relatively low temperature always compromises the barrier properties. The crystals induced by elongational field are too small to serve as barrier unites and the extension of amorphous chains leads to the dedensification of PLA.[36–38]

Taking the above consideration into account, it is still a formidable challenge to put forward a simple and effective strategy for developing high barrier PLA films with desirable ductility at an industrial scale. In the current work, a technology of "biaxial stretching-constrained annealing" was adopted to fabricate PLA films with simultaneously enhanced gas barrier properties and ductility. Biaxial stretching was aimed at constructing an oriented chain entanglement network with small crystals to impart PLA films with superior mechanical performance. Constrained annealing was utilized to facilitate the further growth and perfection of orientated lamellae formed during biaxial stretching, and densify the amorphous chain of PLA, thus suppressing the penetration of diffusion molecules. As a result, the as-prepared PLA films exhibited an impressive comprehensive performance with a low oxygen and water vapor permeability coefficient of 0.733×10^{-14} $cm^3\cdot cm\cdot cm^{-2}\cdot s^{-1}\cdot Pa^{-1}$ and 3.82×10^{-14} $g\cdot cm\cdot cm^{-2}\cdot s^{-1}\cdot Pa^{-1}$, respectively, outstanding ductility with elongation at break of 66.0%, high yield strength of 84.2 MPa, and good transparency of more than 80% at 550 nm. The method proposed herein can overcome the inherent brittleness and insufficient barrier performance of PLA, and is expected to promote the large-scale industrial production and commercial application of high barrier PLA film in the field of packaging materials.

EXPERIMENTAL

Materials

The commercially available PLA film (PLA110) was kindly supplied by Shenghe Plastic Development Co., Ltd., Shandong, China. Sodium hydroxide (NaOH) and methanol were purchased from Chengdu Kelong Chemical Co., Ltd, China, and used as received.

Preparation of PLA films

The commercially available PLA films were produced by sequential biaxial stretching technology, and the stretching directions were denoted as machine direction (MD) and transverse direction (TD), respectively. Constrained annealing is carried out on a high temperature press (LP-S-50, Labtech Engineering, Thailand). The PLA film was annealed with a pressure of 10 MPa for 10 min at 130, 140, 150, 160 °C, respectively. For convenience, the commercially available PLA films before and after constrained annealing were abbreviated as BS-PLA and CA-PLA*x*, where *x* was the temperature during constrained annealing.

Field-Emission Scanning Electronic Microscopy (FE-SEM)

In order to observe the crystalline morphology of BS- and CA-PLA films, all films were immersed in a methanol-water (1:1, *V*:*V*) mixture solution containing NaOH (0.1 $mol\cdot L^{-1}$) for 28 h at room temperature to remove the amorphous phase. Then, the etched samples were cleaned by deionized water with the aid of ultrasonication several times, and dried at 50 °C overnight. The etched surface of PLA films sputter-coated with platinum was observed by FE-SEM (Inspect F, FEI, Finland) under the accelerated voltage of 5 kV.

Dynamic Mechanical Analysis (DMA)

The relaxation of amorphous molecular chains was measured by DMA in tensile mode (Q850, TA instruments, USA). The rectangle sample with a thickness of 50 μm and a width of 8 mm was tested from 40 °C to 120 °C at the heating rate of 3 $°C\cdot min^{-1}$. The frequency and amplitude were fixed at 1 Hz and 15 μm, respectively.

https://doi.org/10.1007/s10118-022-2723-3

Polarized Fourier Transform Infrared Spectroscopy (P-FTIR)

The conformation and orientation of PLA molecular chains were investigated by FTIR equipped with a polaroid (Nicolet 6700, Thermal Scientific, USA). All spectra are collected with a resolution of 4 cm^{-1} and scanning 16 times. A multi-angle scan from 0° to 180° per 10° *via* controlling the polarizers' angle was employed to acquire the orientation information of molecular chain. The dichroic ratio (D) and orientation function (f) were calculated by the equations below:

$$D = A_{\parallel}/A_{\perp} \quad (1)$$

$$f = \frac{D-1}{D+2} \quad (2)$$

where $A_{\parallel}$ and $A_{\perp}$ are the parallel and perpendicular absorbance, respectively.

Differential Scanning Calorimeter (DSC)

The thermal behavior of BS- and CA-PLA films was analyzed by DSC (Q2000, TA instruments). About 5 mg sample was weighed accurately and sealed into aluminum pan waiting for testing. All the samples were heated from 40 °C to 200 °C at a heating rate of 10 °C·min^{-1} under a nitrogen atmosphere. The degree of crystallinity ($X_{c\text{-}DSC}$) can be calculated by equation below.

$$X_{c\text{-}DSC} = \frac{\Delta H_m - \Delta H_{cc}}{\Delta H_m^0} \times 100\% \quad (3)$$

where ΔH_m and ΔH_{cc} are the melting enthalpy and cold crystallization enthalpy, respectively. ΔH_m^0 is the melting enthalpy for the perfect crystal of PLA, which is 93 J·g^{-1}.

Additionally, temperature-modulated DSC (TMDSC) was adopted to ascertain the relaxation of amorphous chains in glass transition region. The underlying heating rate was 2 °C·min^{-1} with a temperature modulation amplitude of 0.318 °C, the oscillation period of 60 s.

Two-dimensional Wide-Angle X-ray Diffraction (2D-WAXD)

2D-WAXD was performed at the beamline BL16B of the Shanghai Synchrotron Radiation Facility (SSRF, China) with the X-ray wavelength of 0.124 nm. 2D-WAXD patterns were collected with an X-ray CCD detector (Pilatus 2M, a resolution of 1475 pixel × 1679 pixel), and the distance from sample to detector was set at 304.0 mm. 1D-WAXD intensity profiles as a function of scatter vector (q) were extracted by integrating the diffraction intensity from the sample patterns in a whole circle (0°–360°) after subtracting the background scattering. The crystallinity ($X_{c\text{-}WAXD}$) was estimated by the following equation:

$$X_{c\text{-}WAXD} = \frac{\sum A_{cryst}}{\sum A_{cryst} + \sum A_{amorp}} \quad (4)$$

where A_{cryst} and A_{amorp} are the fitted diffraction peak areas of lattice planes and amorphous phase, respectively. The mean size of crystal domain (L) was calculated by Scherrer equation:

$$L = K\lambda/B\cos\theta \quad (5)$$

where K=0.89 and B is peak width at half-height of specific lattice planes of PLA.

In addition, the orientation parameter (Herman's orientation factor, f_H) was calculated from the azimuthal scan profiles, which is obtained through integrating the diffraction intensity of specific crystal planes of PLA. The specific equation is listed as follow.

$$f_H = \frac{3\left(\cos^2\varphi\right)_{hkl} - 1}{2} \quad (6)$$

$\cos^2\varphi$ is an orientation factor defined as

$$\cos^2\varphi = \frac{\int_0^{\pi/2} I(\varphi)\cos^2\varphi\sin\varphi d\varphi}{\int_0^{\pi/2} I(\varphi)\sin\varphi d\varphi} \quad (7)$$

where φ is the azimuthal angle and $I(\varphi)$ is the scattering intensity along the angle φ.

Mechanical Performance Testing

The mechanical properties of the BS- and CA-PLA films along both MD and TD at room temperature were tested by a universal testing machine (Model 5576, Instron, USA) with the crosshead speed of 10 mm·min^{-1}. At least five rectangle samples with a length of 50 mm and a width of 10 mm were tested at the same condition for average values and standard deviations.

Gas Barrier Properties Testing

The oxygen permeability measurements were performed using a Gas Permeability Tester (VAC-V2, Labthink instruments, China) at room temperature with 50% of relative humidity according to ISO2556:1974. The water vapor permeability was measured using a Water Vapor Transmission Rate Tester (W3/031, Labthink instruments, China) at 38 °C and 98% relative humidity according to ISO2556:1974. The detailed testing can be observed in our previous work.[17]

Transparency Testing

The transmittance of the BS- and CA-PLA films in visible region was measured by an ultraviolet-visible spectrophotometer (UV-2100, Shimadzu, Japan) with wavelength range from 400–800 nm.

RESULTS AND DISCUSSION

Macroscopic Properties of BS- and CA-PLA Films

For packaging materials, the mechanical performance and gas barrier properties are the essential prerequisites to maintain the quality and safety of the packaged commodities in the processes of storage, transportation, postprocessing and sales.[7,9,39] The transparency is also a valuable feature for visual packaging.[9,40] Next, we will evaluate these three key properties of as-prepared PLA films.

Barrier properties of BS- and CA-PLA films

Fig. 1 summarizes the oxygen permeability (P_{O_2}) and water vapor permeability (P_{H_2O}) of BS- and CA-PLA films. It is observed that the remarkable decrease of P_{O_2} and P_{H_2O} of CA-PLA films with the increase of annealing temperature. Specifically, P_{O_2} of BS-PLA film is only about 2.077×10^{-14} $cm^3\cdot cm\cdot cm^{-2}\cdot s^{-1}\cdot Pa^{-1}$. After constrained annealing, a gradually decreased P_{O_2} of CA-PLA films is achieved with increasing annealing temperature. When the annealing temperature rises up to 160 °C, CA-PLA160 film shows a P_{O_2} of 0.733×10^{-14} $cm^3\cdot cm\cdot cm^{-2}\cdot s^{-1}\cdot Pa^{-1}$, reduced by 62.8% relative to BS-PLA film. Moreover, with the increase annealing temperature, the P_{H_2O} of CA-PLA films is decreased gradually, being in line with the trend of P_{O_2}. Compared with BS-PLA film (8.17×10^{-14} g·cm·$cm^{-2}\cdot s^{-1}\cdot Pa^{-1}$), P_{H_2O} of the CA-PLA films are 5.70, 4.93, 4.21, 3.82×10^{-14} g·cm·$cm^{-2}\cdot s^{-1}\cdot Pa^{-1}$, reduced

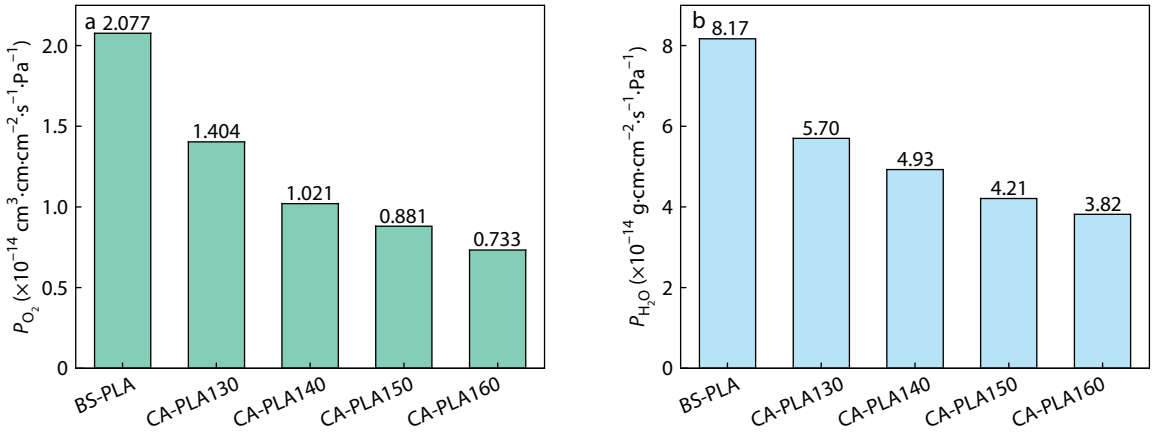

Fig. 1 (a) Oxygen permeability (P_{O_2}) and (b) water vapor permeability (P_{H_2O}) of BS- and CA-PLA films.

by 30.2%, 39.7%, 48.5%, 53.2%, respectively. The oxygen and water barrier properties of CA-PLA films are prominent and comparable to the PET films reported in literature.[41,42] These results demonstrate that the proposed methodology is simple and effective to significantly improve the barrier properties of PLA film without the addition of nanoplatelets or modifiers.

Mechanical performance of BS- and CA-PLA films

Fig. S1 (in the electronic supplementary information, ESI) shows the typical stress-strain curves of BS- and CA-PLA films. As expected, all the PLA films show a ductile fracture behavior and biaxial stretching is beneficial for inducing a brittle-ductile transition, simultaneously enhancing mechanical strength and ductility of PLA film. The detailed mechanical performances including yield strength and elongation at break are summarized in Fig. 2. The yield strength of BS-PLA film in MD and TD is basically the same and the constrained annealing has limited impact on yield strength of CA-PLA films. To be specific, the yield strength of BS- and CA-PLA films except CA-PLA160 is similarly constant, varying slightly in the range of 80-85 MPa in MD and TD. The yield strength of CA-PLA160 film slightly decreases to 71.7 and 76.1 MPa in MD and TD, respectively. More attractively, the impact of constrained annealing on elongation at break is much greater than that on yield strength. As depicted in Fig. 2(b), the elongation at break of CA-PLA films increases first and then decreases with the increase of annealing temperature. The maximum elongation at break of CA-PLA film in TD and MD obtained in the annealing temperature of 130–140 °C is 66.0% and 48.4%, increased by 17.9% and 86.9% relative to BS-PLA film, respectively. When the annealing temperature is up to 160 °C, a substantial reduction in the elongation at break of CA-PLA160 film is seen. It is worth noting that the yield strength and ductility of BS- and CA-PLA films are enhanced significantly in both MD and TD direction compared to traditional cast PLA films. The "biaxial stretching-constrained annealing" strategy is an industrial-scale processing technique to effectively conquer the intrinsic brittleness of PLA film and balance its mechanical strength and ductility without any modifiers.

Transparency of BS- and CA-PLA films

Fig. 3 shows the digital images of BS- and CA-PLA films and their corresponding visible light transmittance spectra in the wavelength range of 400 nm to 800 nm. It is vividly seen that all the films exhibit good transparent to the naked eye, regardless of annealing temperature (Fig. 3a). The quantitative visible light transmittance spectra are shown in Fig. 3(b). With the increase of annealing temperature, the transmittance of CA-PLA films is gradually decreased. All the samples except CA-PLA160 have a high transmittance of above 80% at a wavenumber of 550 nm, which can meet the demand of commercial transparent packaging film.

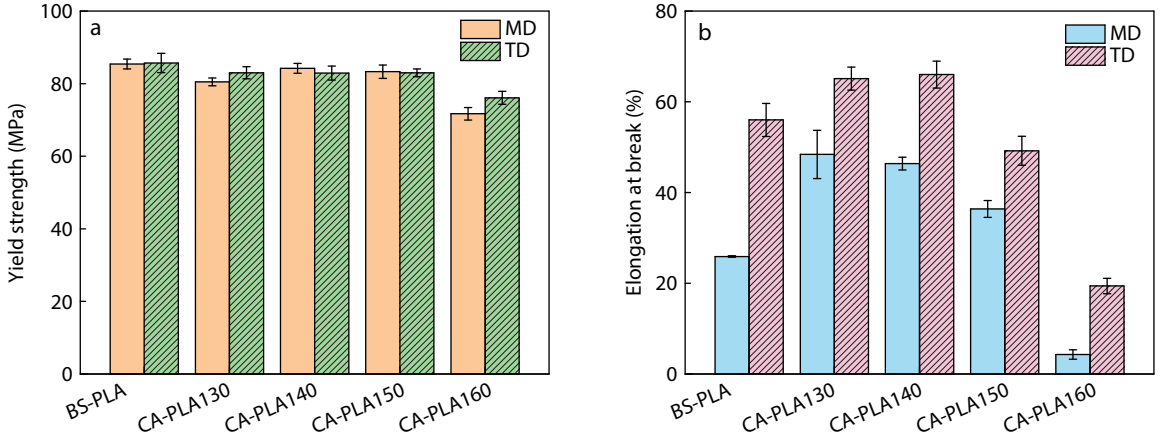

Fig. 2 (a) Yield strength and (b) elongation at break of BS- and CA-PLA films in MD and TD.

https://doi.org/10.1007/s10118-022-2723-3

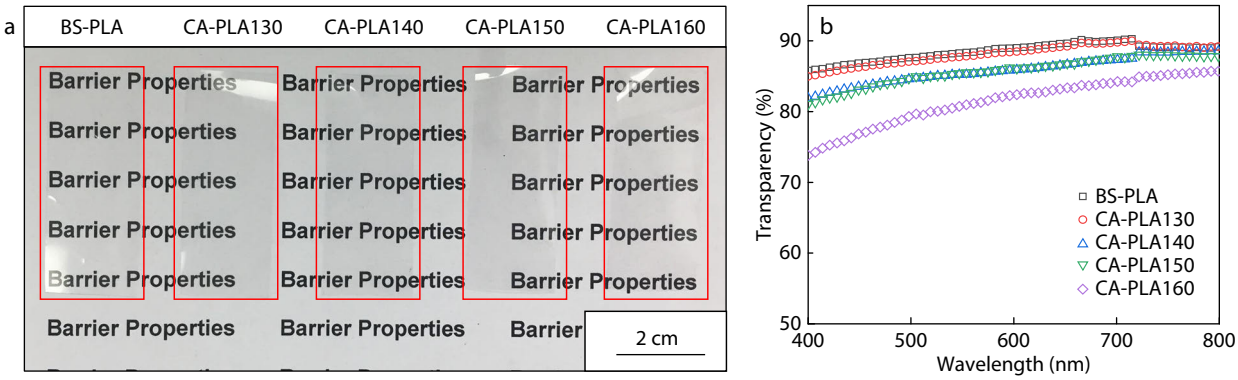

Fig. 3 (a) Digital image and (b) visible light transmittance spectra of BS- and CA-PLA films in the wavelength range of 400–800 nm.

Comprehensive properties of CA-PLA films

As shown in Fig. 4, performance polygon is used to assess the comprehensive properties of CA-PLA films, including oxygen permeability, water permeability, tensile strength, ductility and transparency. Commonly used plastic packaging materials on current market such as biaxial oriented poly(ethylene terephthalate) (BOPET),[41] biaxial oriented polypropylene (BOPP),[43] linear low density polyethylene (LLDPE)[44,45] and high density polyethylene (HDPE)[46] suffer from some distinct shortcomings. To be specific, polyolefin have outstanding ductility and water vapor barrier property but poor oxygen barrier property. As for BOPET, its ductility and water vapor barrier property are not always satisfactory. In comparison with the current petrochemical-based packaging materials, the as-prepared CA-PLA films with unrivalled renewability and biodegradability show excellent comprehensive properties, such as superior gas barrier properties, balanced mechanical performance and good transparent. These merits allow the as-prepared CA-PLA films to be the most promising alternative to replace petrochemical-based packaging materials.

Microscopic Structure of BS- and CA-PLA Films

The highly transparent BS- and CA-PLA films with enhanced gas barrier properties and mechanical performance are closely related to their microscopic structure. To clarify the relationship between microscopic structure and macroscopic performance, it is imperative to shed light on the structural evolution of amorphous chain network and crystalline phase of PLA during biaxial stretching and constrained annealing, which will be shown in the following sections.

Oriented crystalline structure of BS- and CA-PLA films

It is well documented that the crystalline structure plays a critical role in improving the gas barrier properties and mechanical performance, especially for semicrystalline PLA film. In order to explore the origin of the enhancement of barrier properties and mechanical performance, WAXD, SEM and DSC were carried out to characterize the crystalline structure of PLA films during biaxial stretching and constrained annealing.

Fig. 5 displays 2D-WAXD pattern of BA- and CA-PLA films and the corresponding 1D-WAXD curves. We can clearly discern from Figs. 5(a)–5(e) that all the samples exhibit two characteristic diffraction rings assigned to lattice planes (200)/(110) and (203) of PLA crystalline phase[47] and the intensity of characteristic diffraction rings significantly increases with the increase of annealing temperature due to

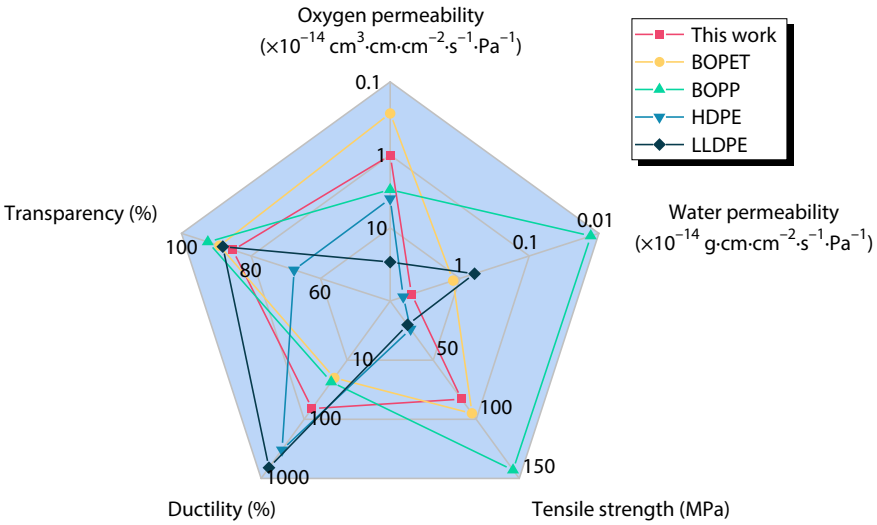

Fig. 4 Performance polygon to evaluate the comprehensive properties of CA-PLA films in comparison to commercial petrochemical-based packaging material in terms of oxygen permeability, water permeability, tensile strength, ductility and transparency.

https://doi.org/10.1007/s10118-022-2723-3

the increased crystallinity. The 1D-WAXD intensity profiles in Fig. 5(f) represent the diffraction peaks at q value of 10.5, 11.8, 13.5, 15.8, which are empirically regarded as the lattice plane (010), (200)/(110), (203), (015) of PLA α-form crystal.[27,48,49] Note that the characteristic diffraction peaks assigned to the lattice plane (010) and (015) are absent in the BS-PLA film, while the lattice plane (200)/(110), (203) and (206)/(106) shift slightly toward lower q value. This result indicates that biaxial stretching induces considerable disordered α' form in the BS-PLA film.[48,50–52] With increasing the annealing temperature, the enhanced intensity of all diffraction peaks are accompanied with the emergence of new diffraction peaks marked asterisk assigned to the orthorhombic α form, and the peak assigned to lattice plane (200)/(110) splits into two peaks that can be clearly seen in Fig. 5(f). It should be attributed to the thermal-induced transition from α' form to α form during constrained annealing. This conclusion is also confirmed by DSC results in Fig. S2 (in ESI). Besides, crystallinity and the mean size of crystal domain are listed in Table 1. It is taken for granted that thermal annealing is beneficial for the perfection of crystalline structure formed in the BS-PLA film, thus increasing the crystallinity and crystal size. To be Specific, constrained annealing boosts up the crystallinity from 26.9% for BS-PLA film to 40.5% for CA-PLA160 film. The same variation tendency of crystallinity is also seen by DSC results. Correspondingly, the size of crystal domain, *i.e.*, L_{hkl} value, gradually increases from 26.3 nm for BS-PLA film to 32.1 nm for CA-PLA160 film.

As shown in 2D-WAXD patterns, the strong diffraction arcs around meridian indicate the orientation of crystal. The azimuthal profiles of WAXD are presented in Fig. 5(g) and the corresponding orientation parameters (Herman's orientation factor, f_H) are summarized in Table 1. It is obvious that f_H increases after constrained annealing. It suggests that the crystalline phase of as-prepared PLA film is in-plane anisotropic. For BS-PLA film, abundant oriented crystal nuclei are induced by intensive stretching stress. However, the disordered α' form is the dominant crystalline phase and BS-PLA film represents a relatively low value of f_H. After constrained annealing, the oriented crystal nuclei induce perfect oriented crystal further, leading to the increase of f_H. This result is in line with the SEM observation of oriented crystalline morphology, as shown in Fig. S3 (in ESI).

Amorphous molecular conformation of BS- and CA-PLA films

Apart from crystalline structure, amorphous molecular conformation of semicrystalline PLA also has a great influence on the macroscopic properties.[26,53] During biaxial stretching and constrained annealing, the amorphous molecular chain network changes significantly in response to the external field. Herein, DMA is adopted to supply more information about amorphous molecular chain. As shown in Fig. 6(a), the loss modulus with a peak value of 390 MPa for BS-PLA film is observed at 73 °C, *i.e.*, T_g, which is obviously higher than that of unoriented PLA film. This is attributed to the multiple amorphous chain entanglement network formed during biaxial stretching.[54] After constrained annealing at 130–140 °C, a broader loss modulus peaks with lower peak value shift higher temperature relative to BS-PLA film, which is further confirmed by the weaker glass transition signals in TMDSC (Fig. 6b). When the annealing temperature is as high as 150–160 °C, the loss modulus peaks with lower peak value shift to lower temperature relative to BS-PLA films. It is interesting that the loss modulus peak becomes narrower for CA-PLA160. It can be concluded that due to the perfection of crystal, the restricted amorphous molecular chains are consumed and the

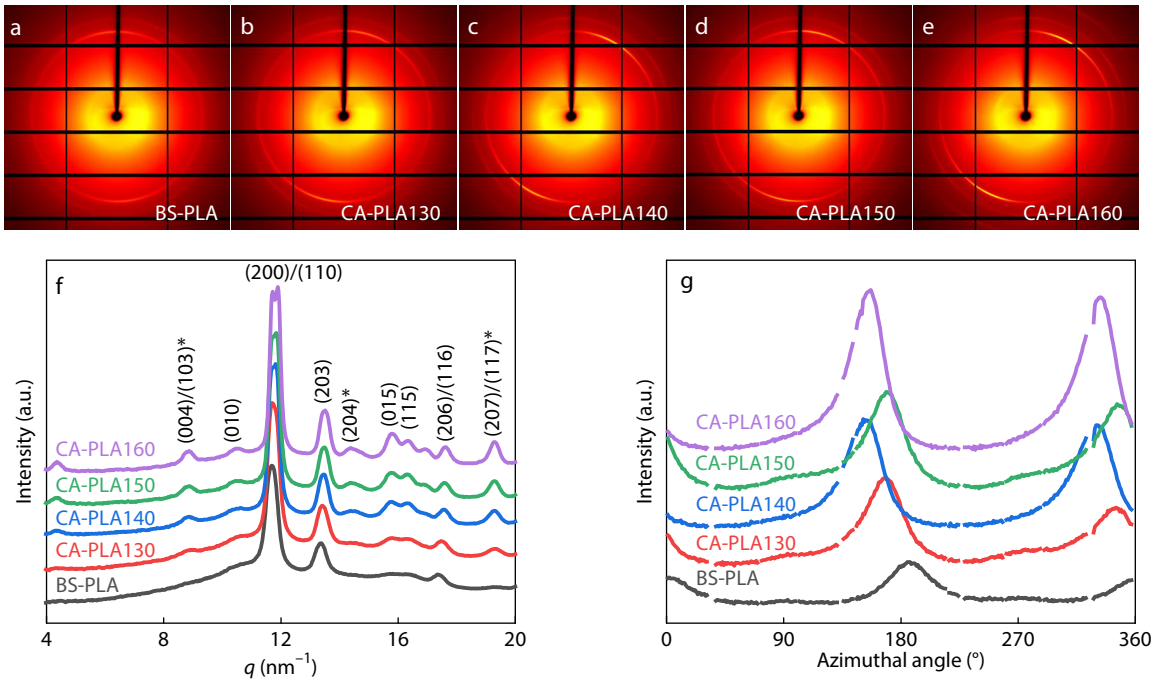

Fig. 5 (a–e) 2D-WAXD patterns, (f) one-dimensional-WAXD diffraction profiles and (g) intensity distribution of (200/110) reflection of BS- and CA-PLA films along the azimuthal angle from 0° to 360°.

https://doi.org/10.1007/s10118-022-2723-3

Table 1 Structure parameter in crystalline region of BS- and CA-PLA films including crystallinity, crystal size, Herman's orientation factor and melting temperature summarized from WAXD and DSC results.

Sample	$X_{c\text{-}WAXD}$ (%)	L_{hkl} (nm)	f_H	$X_{c\text{-}DSC}$ (%)	T_m (°C)
BS-PLA	26.9	23.8	0.103	51.5	171.4
CA-PLA130	32.1	26.3	0.184	52.5	171.0
CA-PLA140	36.7	28.9	0.292	55.2	171.5
CA-PLA150	38.8	29.9	0.242	62.8	171.3
CA-PLA160	40.5	32.1	0.366	70.9	173.9

entanglements are reduced, resulting in the enhancement on their mobility and relaxation. On the basis of WAXD results, we speculate that the constrained annealing has two effects on the amorphous molecular conformation. On one hand, the formation of nano-sized crystals during constrained annealing can act as physical crosslink to strengthen the amorphous chain entanglement network. On the other hand, the amorphous chain entanglement network will be weakened if excessive amorphous molecular chains are consumed due to the thermal annealing induced crystallization. These two effects compete with each other during constrained annealing. The former effect is dominant to obtain reinforced chain entanglement network at annealing temperature of 130–140 °C, while the latter effect becomes a dominant factor in constructing more perfect PLA crystals with increased crystallinity at higher annealing temperature of 150–160 °C.

The wavenumber and intensity of characteristic band of FTIR spectra are highly sensitive to the conformation and local molecular environment of polymers. Herein, P-FTIR spectroscopy is carried out to further reflect the molecular conformation of PLA during biaxial-stretching and constrained annealing. Fig. S4 (in ESI) depicts the infrared spectra of BS- and CA-PLA films with angle of polarization from 0° to 180°. It is vividly seen that two bands at 921 and 956 cm^{-1} are undulating with the variation of polarized angle. For PLA, the characteristic absorption band at 921 cm^{-1} is assigned to the coupling of the C—C backbone stretching and —CH_3 rocking vibration, which is sensitive to the 10_3 helical conformation of crystalline region, while the characteristic absorption band at 956 cm^{-1} is generally attributed to the —CH_3 rocking vibration of PLA chains in the amorphous region.[55–58] Hence the characteristic absorption bands at 921 and 956 cm^{-1} are used to calculate the degree of orientation in crystalline region (f_c) and amorphous region (f_a).[59] The change in intensity of absorption bands at 921 and 956 cm^{-1} as a function of polarization angle is collected in Figs. 7(a)–7(e)**.** It can be seen that both BS- and CA-PLA films represent oval shapes that are elongated gradually with the increase of annealing temperature, implying the increased orientation of the amorphous and crystalline regions. In addition, the polarization angle of crystalline region in maximum absorption is perpendicular to that of amorphous region. This is indicative of the same orientation direction of PLA molecular chains in the amorphous and crystalline regions.[60] Furthermore, the orientation factors are quantitatively calculated and summarized in Fig. 7(f). It can be observed that f_c increases with the increase of annealing temperature, which agrees with f_H calculated from WAXD. Meanwhile, f_a increases sharply when the annealing temperature below 140 °C, and then it gradually levels off when the annealing temperature is above 150 °C. The variation identifies with the results of DMA. It can be inferred that the molecular chains in amorphous region are oriented along the direction of chain packing in lamellae due to the confinement of oriented lamellae.

Origin of the Enhanced Gas Barrier and Mechanical Properties

The excellent gas barrier and mechanical properties of PLA films are closely related to the robust amorphous chain entanglement network and oriented lamellar structure formed during biaxial stretching and constrained annealing. The new insight into PLA microscopic structure including crystalline and amorphous phases and their relationship with macroscopic properties is conductive to our understanding of the mechanism of the advanced barrier and mechanical properties of PLA films, thus providing a significant guidance for the large-scale production of PLA films with excellent comprehensive performance. The structure evolution of both amorphous and crystalline region in PLA films during biaxial stretching and constrained annealing is schematically illustrated in Fig. 8. According to the amorphous and crystalline structural analysis of BS- and CA-PLA films, the oriented amorphous chain entanglement network and nano-sized lamellae are formed during biaxial stretching. After constrained annealing at 130 and 140 °C, the oriented amorphous chain entanglement network

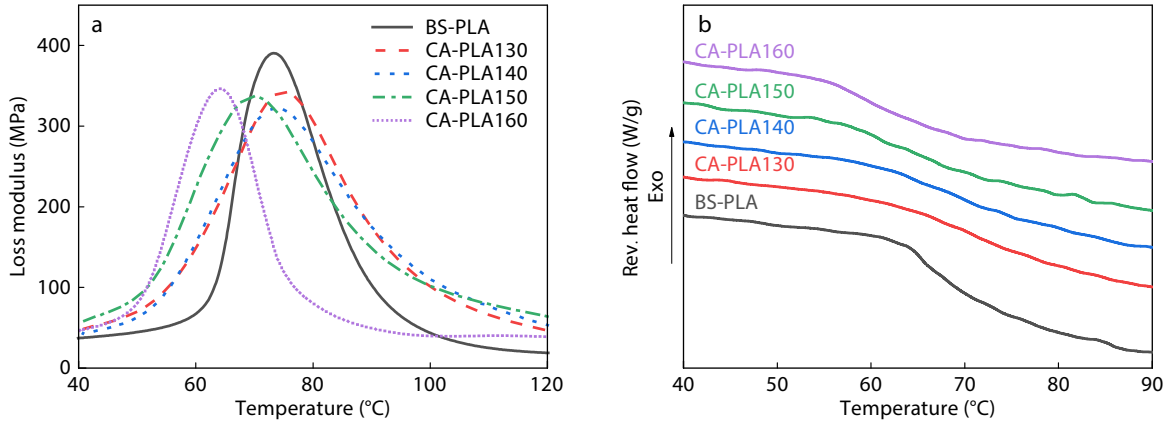

Fig. 6 (a) Loss modulus and (b) reversible heat flow curves of BS- and CA-PLA films.

https://doi.org/10.1007/s10118-022-2723-3

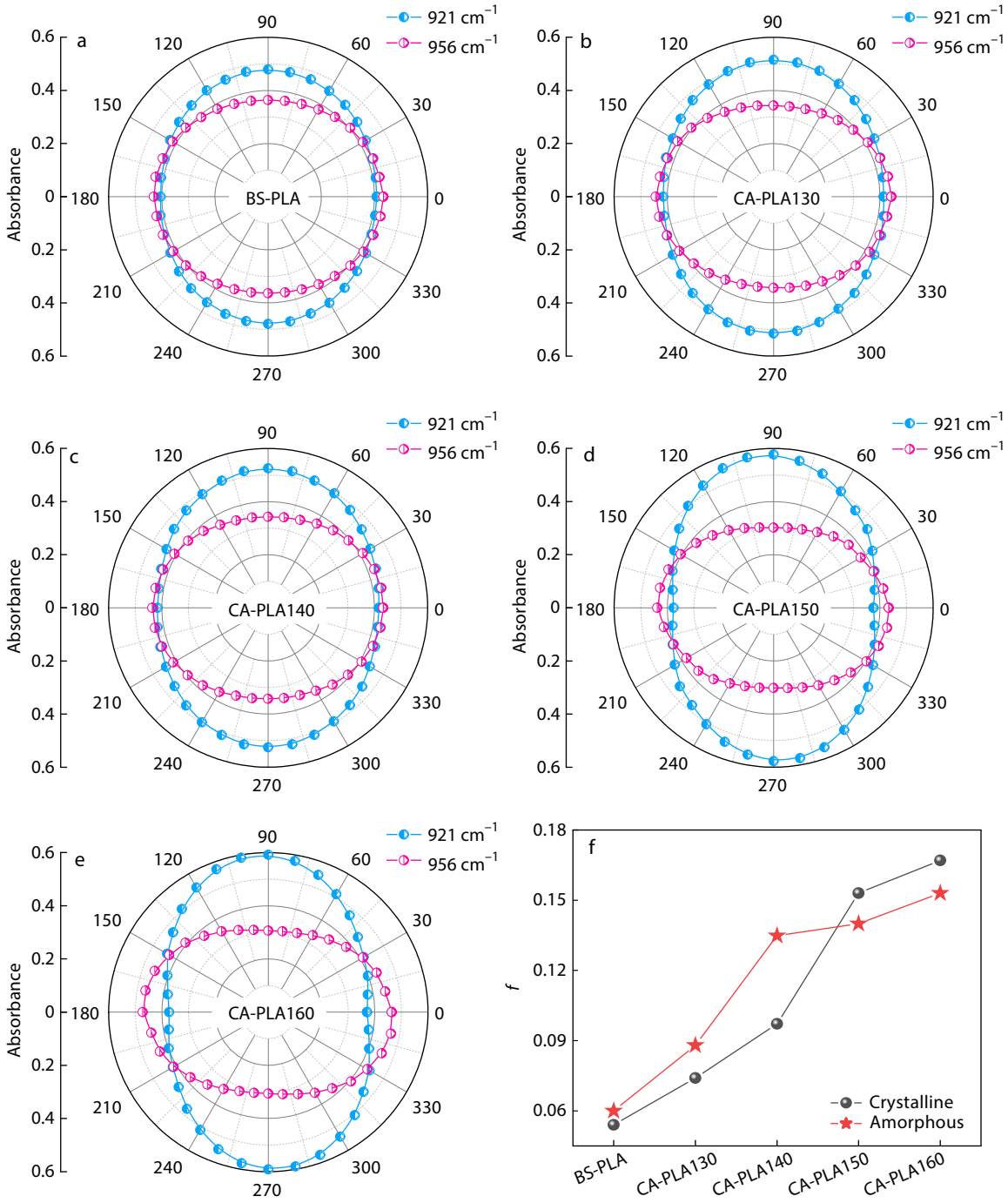

Fig. 7 (a–e) The absorbance of P-FTIR absorption bands at 921 and 956 cm^{-1} with angle of polarization from 0° to 360°; (f) Calculated orientation factors of 956 cm^{-1} (f_a) and 921 cm^{-1} (f_a) as a function of annealing temperature.

and crystal of CA-PLA films are further strengthened. On the one hand, the small orientated crystal nuclei induced by biaxial stretching and the *α′* form with loose packing is transformed into *α* form, leading to the increase of crystallinity and crystalline orientation. On the other hand, the oriented lamellae can serve as physical crosslink to strengthen the amorphous chain entanglement network, and restrict the relaxation of amorphous molecular, thus, improving the amorphous orientation. When the constrained annealing temperature rises up to 150 and 160 ℃, it is expected that the crystal size increases further and more perfect *α* form crystals are formed due to high movement activity of PLA molecular chains. As a result, abundant amorphous molecular chains are consumed and considerable amorphous chain entanglement network is weakened.

In order to further clarify the relationship between the microscopic structure of PLA films and their barrier properties, the barrier mechanism is discussed in detail. Fig. 9(a) depicts

https://doi.org/10.1007/s10118-022-2723-3

the oxygen pressure variations in the downstream compartment as a function of the reduced time, displaying a typical time lag permeation curve. As annealing temperature elevates, the delay time (nonlinear region) increases slightly, suggesting that the dissolution process becomes more laborious. And the slope of the subsequent linear region gradually decreases, demonstrating a more difficult diffusion process of oxygen molecule. The corresponding diffusion (*D*) and solubility (*S*) coefficients are extracted in Fig. 9(b). It can be observed that both *D* and *S* decrease with the increase of annealing temperature, being consistent with the previous interpretation of permeation behavior of oxygen. Taking the structural evolution of PLA films into consideration, it can be inferred that there are two main reasons for the significant improvement of gas barrier properties of CA-PLA films. First, the oriented PLA lamellae with nano-sized and perfect structure formed during constrained annealing can serve as "nano-barrier wall",[22] giving rise to more tortuous penetration paths for diffusing molecules, as shown in Fig. 8. Second, because the dissolution of gas molecule almost occurs in amorphous phase for semicrystalline PLA,[20] the increase of crystallinity and the densification of amorphous molecular chains diminish the free volume effectively, leading to an increase in the residence time of diffusion molecules. Thus, the synchronous decline in *D* and *S* allows the considerable improvement of gas barrier performance for CA-PLA films.

As for mechanical performance, the superior yield strength and ductility of BS-PLA film originate from the oriented nano-sized lamellae and robust amorphous chain entanglement network. As previously mentioned, the small size lamellae can serve as physical crosslink to enhance the amorphous chains entanglement network, resulting in the improvement of ductility without sacrificing strength.[26] According to the structural evolution of CA-PLA films depicted in Fig. 8, the influence of constrained annealing on ductility can be divided into two stages. When annealing temperature is below 140 °C, it can be inferred that amorphous chain entanglement network is well strengthened by the well-defined nano-sized lamellae, exhibiting significantly enhanced ductility of CA-PLA films. However, once annealing temperature rises above 150 °C, the further growth and perfection of crystallites result in the increased defects between crystallites and excessive consumption of amorphous chains weakens amorphous chain entanglement network. Therefore, the ductility of CA-PLA films deteriorates inevitably.

With the well-defined nano-sized crystals and robust

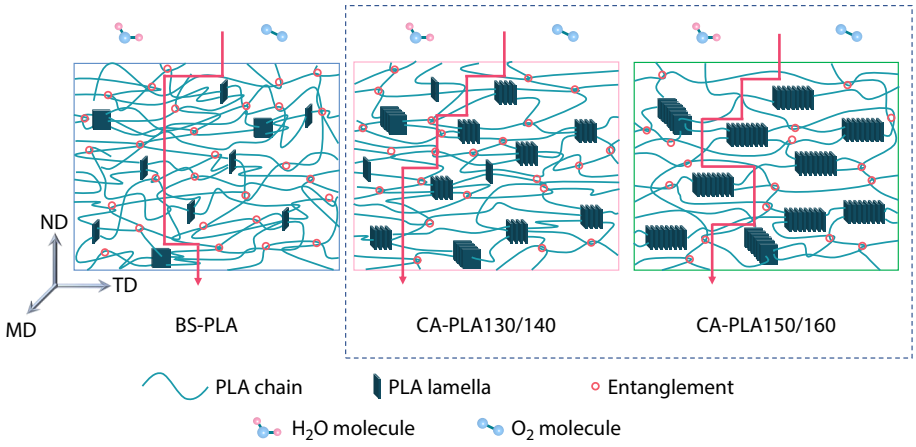

Fig. 8 Schematic illustration of the structure evolution of amorphous and crystalline region for PLA films during biaxial stretching and constrained annealing.

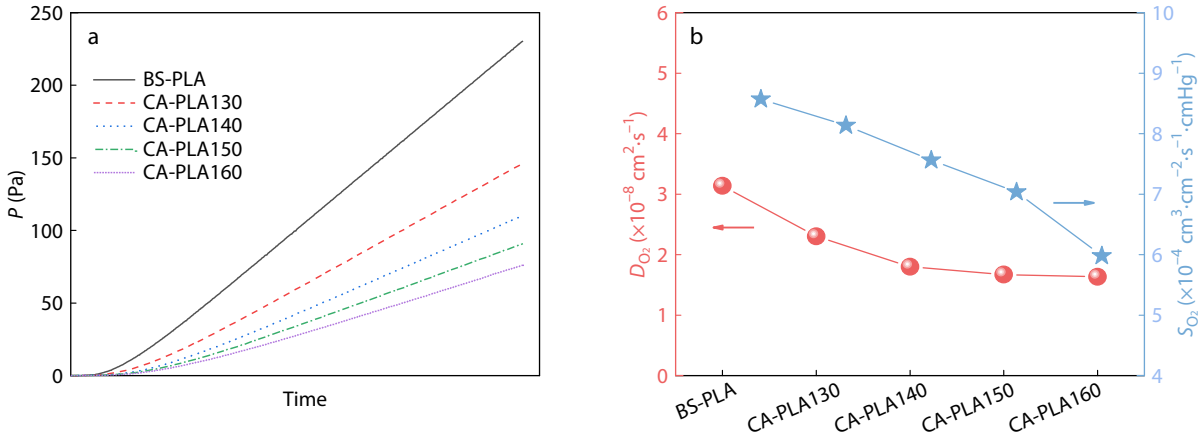

Fig. 9 (a) O_2 pressure variations in the downstream compartment as a function of the reduced time; (b) Diffusion (D_{O_2}) and solubility (S_{O_2}) coefficients of BS- and CA-PLA films.

https://doi.org/10.1007/s10118-022-2723-3

amorphous chain entanglement network during biaxial stretching and constrained annealing, it is conceivable that the barrier properties and ductility of PLA films are simultaneously enhanced. The results represented here provide an in-depth understanding the relationship between microscopic structure and macroscopic performance, which has a significant guidance for developing high barrier PLA films with superior ductility at an industrial scale. Nevertheless, it is still a formidable challenge to quantitatively characterize amorphous chain entanglement network.[54] Much efforts should be taken to regulate crystalline and amorphous structure for controlling the macroscopic performance of semicrystalline PLA films.

CONCLUSIONS

A simple but effective method of "biaxial stretching-constrained annealing" was employed to improve the gas barrier properties and ductility of PLA films in this work. The microscopic structure including crystalline and amorphous phases of the as-prepared PLA film was evaluated by WAXD, SEM, TMDSC, DMA and P-FTIR characterizations. On the basis of crystalline structure analyses, it could be concluded that the perfect oriented lamellae could serve as "nano-barrier wall" to build a tortuous pathway and densify the stacking of molecular chains, thus suppressing the diffusion and dissolution processes of diffusing molecules in the PLA films. Moreover, the nano-sized crystallites formed during constrained annealing could be taken as physical crosslink to reinforce the chain entanglement network and improve the ductility of PLA films. As a result, the P_{O_2} of CA-PLA films can be reduced more than 50% compared with that of BS-PLA film, while the elongation at break is improved more than 79% in MD and 17% in TD. Additionally, as-prepared PLA films have a high transmittance of above 80% in the visible light wavelength range. The proposed methodology of biaxial stretching and constrained annealing is hopeful to be applied in scalable industrial production to simultaneously enhance the gas barrier and mechanical properties of PLA films. The understanding of the relationship between microscopic structure and macroscopic properties of PLA films is necessary for developing biodegradable PLA materials with high performance, thus broadening their application field to replace conventional undegradable fossil-based plastics.

NOTES

The authors declare no competing financial interest.

Electronic Supplementary Information

Electronic supplementary information (ESI) is available free of charge in the online version of this article at http://doi.org/10.1007/s10118-022-2723-3.

ACKNOWLEDGMENTS

This work was financially supported by the National Key Research and Development Program of China (No. 2018YFB0704200), the National Natural Science Foundation of China (Nos. 51803140, 52033005, 51822305 and 21776186), the Science and Technology Department of Sichuan Province (No. 2018JY0584), the Postdoctoral Science Foundation of China (No. 2019M663496), and the State Key Laboratory of Polymer Materials Engineering (No. sklpme2021-4-03). We also thank Beamline 16B in Shanghai Synchrotron Radiation Facility (SSRF) for supporting the X-ray measurement.

REFERENCES

1 Zhang, Q. N.; Song, M. Z.; Xu, Y. N.; Wang, W. C.; Wang, Z.; Zhang, L. Q. Bio-based polyesters: recent progress and future prospects. *Prog. Polym. Sci.* **2021**, *120*, 101430.
2 Wu, F.; Misra, M.; Mohanty, A. K. Challenges and new opportunities on barrier performance of biodegradable polymers for sustainable packaging. *Prog. Polym. Sci.* **2021**, *117*, 101395.
3 Divakara Shetty, S.; Shetty, N. Investigation of mechanical properties and applications of polylactic acids—a review. *Mater. Res. Express* **2019**, *6*, 112002.
4 Castro-Aguirre, E.; Iniguez-Franco, F.; Samsudin, H.; Fang, X.; Auras, R. Poly(lactic acid)-mass production, processing, industrial applications, and end of life. *Adv. Drug Deliv. Rev.* **2016**, *107*, 333–366.
5 Farah, S.; Anderson, D. G.; Langer, R. Physical and mechanical properties of PLA, and their functions in widespread applications—a comprehensive review. *Adv. Drug Deliv. Rev.* **2016**, *107*, 367–392.
6 Lim, L. T.; Auras, R.; Rubino, M. Processing technologies for poly(lactic acid). *Prog. Polym. Sci.* **2008**, *33*, 820–852.
7 Malinconico, M. ; Vink, E. T. H. ; Cain, A. *Applications of poly(lactic acid) in commodities and specialties. in industrial applications of poly(lactic acid)*, Di Lorenzo, M. ; Androsch, R. , Eds. Springer, Cham: **2018**; pp. 35–50.
8 Risyon, N. P.; Othman, S. H.; Basha, R. K.; Talib, R. A. Characterization of polylactic acid/halloysite nanotubes bionanocomposite films for food packaging. *Food Packag. Shelf Life* **2020**, *23*, 100450.
9 Auras, R.; Harte, B.; Selke, S. An overview of polylactides as packaging materials. *Macromol. Biosci.* **2004**, *4*, 835–864.
10 Liu, R. Y. F.; Schiraldi, D. A.; Hiltner, A.; Baer, E. Oxygen-barrier properties of cold-drawn polyesters. *J. Polym. Sci. , Part B: Polym. Phys.* **2002**, *40*, 862–877.
11 Razavi, M.; Cheng, S. W.; Huang, D.; Zhang, S. F.; Wang, S. Q. Crazing and yielding in glassy polymers of high molecular weight. *Polymer* **2020**, *197*, 122445.
12 Wang, J.; Gardner, D. J.; Stark, N. M.; Bousfield, D. W.; Tajvidi, M.; Cai, Z. Moisture and oxygen barrier properties of cellulose nanomaterial-based films. *ACS Sustain. Chem. Eng* **2017**, *6*, 49–70.
13 Auras, R. A.; Harte, B.; Selke, S.; Hernandez, R. Mechanical, physical, and barrier properties of poly(lactide) films. *J. Plast. Film Sheeting* **2003**, *19*, 123–135.
14 Sonchaeng, U.; Iñiguez-Franco, F.; Auras, R.; Selke, S.; Rubino, M.; Lim, L. T. Poly(lactic acid) mass transfer properties. *Prog. Polym. Sci.* **2018**, *86*, 85–121.
15 Cui, Y.; Kundalwal, S. I.; Kumar, S. Gas barrier performance of graphene/polymer nanocomposites. *Carbon* **2016**, *98*, 313–333.
16 Cui, Y.; Kumar, S.; Rao Kona, B.; van Houcke, D. Gas barrier properties of polymer/clay nanocomposites. *RSC Adv.* **2015**, *5*, 63669–63690.
17 Li, L.; Zhou, Z. H.; Yang, B.; Ji, X.; Huang, H. D.; Zhong, G. J.; Xu, L.; Li, Z. M. Robust cellulose nanocomposite films based on covalently cross-linked network with effective resistance to water

permeability. *Carbohydr. Polym.* **2019**, *211*, 237–248.
18 Xu, P. P.; Zhang, S. M.; Huang, H. D.; Xu, L.; Zhong, G. J.; Li, Z. M. Highly efficient three-dimensional gas barrier network for biodegradable nanocomposite films at extremely low loading levels of graphene oxide nanosheets. *Ind. Eng. Chem. Res.* **2020**, *59*, 5818–5827.
19 Huang, H.-D.; Ren, P.-G.; Xu, J.-Z.; Xu, L.; Zhong, G. J.; Hsiao, B. S.; Li, Z. M. Improved barrier properties of poly(lactic acid) with randomly dispersed graphene oxide nanosheets. *J. Membr. Sci.* **2014**, *464*, 110–118.
20 Huang, H. D.; Zhou, S. Y.; Zhou, D.; Ren, P. G.; Xu, J. Z.; Ji, X.; Li, Z. M. Highly efficient "composite barrier wall" consisting of concentrated graphene oxide nanosheets and impermeable crystalline structure for poly(lactic acid) nanocomposite films. *Ind. Eng. Chem. Res.* **2016**, *55*, 9544–9554.
21 Bai, H.; Huang, C.; Xiu, H.; Zhang, Q.; Deng, H.; Wang, K.; Chen, F.; Fu, Q. Significantly improving oxygen barrier properties of polylactide *via* constructing parallel-aligned shish-kebab-like crystals with well-interlocked boundaries. *Biomacromolecules* **2014**, *15*, 1507–1514.
22 Zhou, S. Y.; Huang, H. D.; Ji, X.; Yan, D. X.; Zhong, G. J.; Hsiao, B. S.; Li, Z. M. Super-robust polylactide barrier films by building densely oriented lamellae incorporated with ductile *in situ* nanofibrils of poly(butylene adipate-*co*-terephthalate). *ACS Appl. Mater. Interfaces* **2016**, *8*, 8096–8109.
23 Kakroodi, A. R.; Kazemi, Y.; Nofar, M.; Park, C. B. Tailoring poly(lactic acid) for packaging applications *via* the production of fully bio-based *in situ* microfibrillar composite films. *Chem. Eng. J.* **2017**, *308*, 772–782.
24 Zhou, S. Y.; Huang, H. D.; Xu, L.; Yan, Z.; Zhong, G. J.; Hsiao, B. S.; Li, Z. M. *In situ* nanofibrillar networks composed of densely oriented polylactide crystals as efficient reinforcement and promising barrier wall for fully biodegradable poly(butylene succinate) composite films. *ACS Sustain. Chem. Eng.* **2016**, *4*, 2887–2897.
25 Gao, X. R.; Li, Y.; Huang, H.-D.; Xu, J. Z.; Xu, L.; Ji, X.; Zhong, G. J.; Li, Z. M. Extensional stress-induced orientation and crystallization can regulate the balance of toughness and stiffness of polylactide films: interplay of oriented amorphous chains and crystallites. *Macromolecules* **2019**, *52*, 5278–5288.
26 Razavi, M. ; Wang, S. Q. Why is crystalline poly(lactic acid) brittle at room temperature? *Macromolecules* **2019**, *52*, 5429–5441.
27 Ou, X.; Cakmak, M. Comparative study on development of structural hierarchy in constrained annealed simultaneous and sequential biaxially stretched polylactic acid films. *Polymer* **2010**, *51*, 783–792.
28 Ou, X.; Cakmak, M. Influence of biaxial stretching mode on the crystalline texture in polylactic acid films. *Polymer* **2008**, *49*, 5344–5352.
29 Xu, S.; Tahon, J. F.; De-Waele, I.; Stoclet, G.; Gaucher, V. Brittle-to-ductile transition of PLA induced by macromolecular orientation. *Express Polym. Lett.* **2020**, *14*, 1034–1047.
30 Zhou, H. W.; Song, Z. Q.; Cai, S. Q. Toughening of poly(lactide acid) with low crystallinity through biaxial poststretching. *J. Polym. Sci.* **2020**, *58*, 3488–3495.
31 Winotapun, C.; Kerddonfag, N.; Daud, W.; Chinsirikul, W.; Takarada, W.; Kikutani, T. Effect of biaxial-simultaneous stretching conditions on OTR and CO_2 permeation of CO_2 laser perforated poly(lactic acid) film. *Packag. Technol. Sci.* **2018**, *31*, 545–556.
32 Jariyasakoolroj, P.; Tashiro, K.; Wang, H.; Yamamoto, H.; Chinsirikul, W.; Kerddonfag, N.; Chirachanchai, S. Isotropically small crystalline lamellae induced by high biaxial-stretching rate as a key microstructure for super-tough polylactide film. *Polymer* **2015**, *68*, 234–245.
33 Al-Itry, R.; Lamnawar, K.; Maazouz, A.; Billon, N.; Combeaud, C. Effect of the simultaneous biaxial stretching on the structural and mechanical properties of PLA, PBAT and their blends at rubbery state. *Eur. Polym. J.* **2015**, *68*, 288–301.
34 Tabatabaei, S. H.; Ajji, A. Crystal structure and orientation of uniaxially and biaxially oriented PLA and PP nanoclay composite films. *J. Appl. Polym. Sci.* **2011**, 4854–4863.
35 Tsai, C. C.; Wu, R. J.; Cheng, H. Y.; Li, S. C.; Siao, Y. Y.; Kong, D. C.; Jang, G. W. Crystallinity and dimensional stability of biaxial oriented poly(lactic acid) films. *Polym. Degrad. Stabil.* **2010**, *95*, 1292–1298.
36 Kanehashi, S.; Kusakabe, A.; Sato, S.; Nagai, K. Analysis of permeability; solubility and diffusivity of carbon dioxide; oxygen; and nitrogen in crystalline and liquid crystalline polymers. *J. Membr. Sci.* **2010**, *365*, 40–51.
37 Drieskens, M.; Peeters, R.; Mullens, J.; Franco, D.; Lemstra, P. J.; Hristova-Bogaerds, D. G. Structure versus properties relationship of poly(lactic acid). I. Effect of crystallinity on barrier properties. *J. Polym. Sci., Part B: Polym. Phys.* **2009**, *47*, 2247–2258.
38 Colomines, G.; Ducruet, V.; Courgneau, C.; Guinault, A.; Domenek, S. Barrier properties of poly(lactic acid) and its morphological changes induced by aroma compound sorption. *Polym. Int.* **2010**, *59*, 818–826.
39 Domenek, S.; Fernandes-Nassar, S.; Ducruet, V. Rheology, mechanical properties, and barrier properties of poly(lactic acid). In *Synthesis, Structure and Properties of Poly(lactic acid)*, Springer, **2017**, pp. 303–341.
40 Kim, T.; Tran, T. H.; Hwang, S. Y.; Park, J.; Oh, D. X.; Kim, B. S. Crab-on-a-tree: all biorenewable, optical and radio frequency transparent barrier nanocoating for food packaging. *ACS Nano* **2019**, *13*, 3796–3805.
41 Gao, H.; Cao, W.; He, J.; Bai, Y. Highly transparent biaxially oriented poly(ester amide) film with improved gas barrier properties and good mechanical strength. *Eur. Polym. J.* **2021**, *156*, 110620.
42 Zekriardehani, S.; Joshi, A. S.; Jabarin, S. A.; Gidley, D. W.; Coleman, M. R. Effect of dimethyl terephthalate and dimethyl isophthalate on the free volume and barrier properties of poly(ethylene terephthalate) (PET): amorphous PET. *Macromolecules* **2018**, *51*, 456–467.
43 Zhang, M.; Li, D.; Xu, W.; Chang, H.; Liu, Q.; Fu, Y.; Liao, R.; Shi, J.; Wang, Y.; He, X. Crystalline structure and morphology of biaxially oriented polypropylene film under the coexistence of organic silica particles and its influence on the adsorption diffusion of polar solvent molecules. *Packag. Technol. Sci.* **2019**, *32*, 75–84.
44 Bumbudsanpharoke, N.; Wongphan, P.; Promhuad, K.; Leelaphiwat, P.; Harnkarnsujarit, N. Morphology and permeability of bio-based poly(butylene adipate-*co*-terephthalate) (PBAT), poly(butylene succinate) (PBS) and linear low-density polyethylene (LLDPE) blend films control shelf-life of packaged bread. *Food Control* **2022**, *132*, 108541.
45 Deng, J.; Chen, Q. J.; Chen, D. J.; Zheng, L. J.; Li, W.; Wang, J. H.; Wang, X. L.; Wei, Y. C.; Chen, Z.; Chen, S.; Sun, K. Q.; Zhang, J. Y.; Ding, Q. M.; Liu, D. M.; Fu, X. J. Nano-titanium dioxide/basic magnesium hypochlorite-containing linear low-density polyethylene composite film on food packaging application. *Mater. Express* **2020**, *10*, 771–779.
46 Ma, Z. L.; Tsou, C. H.; Yao, Y. L.; De Guzman, M. R.; Wu, C. S.; Gao, C.; Yang, T.; Chen, Z. J.; Zeng, R.; Li, Y.; Yang, T. T.; Wang, P.; Lin, L. Thermal properties and barrier performance of antibacterial high-density polyethylene reinforced with carboxyl graphene-grafted modified high-density polyethylene. *Ind. Eng. Chem. Res.* **2021**, *60*, 12911–12922.
47 Xiang, S.; Jun, S.; Li, G.; Bian, X. C.; Feng, L. D.; Chen, X. S.; Liu, F. Q.; Huang, S. Y. Effects of molecular weight on the crystallization and melting behaviors of poly(L-lactide). *Chinese J. Polym. Sci.* **2016**, *34*, 69–76.

https://doi.org/10.1007/s10118-022-2723-3

48 Pan, P.; Kai, W.; Zhu, B.; Dong, T.; Inoue, Y. Polymorphous crystallization and multiple melting behavior of poly(L-lactide): molecular weight dependence. *Macromolecules* **2007**, *40*, 6898–6905.
49 Li, X. J.; Zhong, G. J.; Li, Z. M. Non-isothermal crystallization of poly(L-lactide) (PLLA) under quiescent and steady shear conditions. *Chinese J. Polym. Sci.* **2010**, *28*, 357–366.
50 Stoclet, G.; Seguela, R.; Lefebvre, J. M.; Elkoun, S.; Vanmansart, C. Strain-induced molecular ordering in polylactide upon uniaxial stretching. *Macromolecules* **2010**, *43*, 1488–1498.
51 Righetti, M. C.; Gazzano, M.; Di Lorenzo, M. L.; Androsch, R. Enthalpy of melting of *α*′- and *α*-crystals of poly(L-lactic acid). *Eur. Polym. J.* **2015**, *70*, 215–220.
52 Hu, J.; Wang, J.; Gowd, E. B.; Yuan, Y.; Zhang, T.; Duan, Y.; Hu, W.; Zhang, J. Small- and wide-angle X-ray scattering study on *α*′-to-*α* transition of poly(L-lactide acid) crystals. *Polymer* **2019**, *167*, 122–129.
53 Xu, P. P.; Yang, S.; Gao, X. R.; Chen, S. P.; Xu, L.; Zhong, G. J.; Huang, H. D.; Li, Z. M. Constructing robust chain entanglement network, well-defined nanosized crystals and highly aligned graphene oxide nanosheets: Towards strong, ductile and high barrier poly(lactic acid) nanocomposite films for green packaging. *Compos. Part B-Eng.* **2021**, *222*, 109048.
54 Delpouve, N.; Delbreilh, L.; Stoclet, G.; Saiter, A.; Dargent, E. Structural dependence of the molecular mobility in the amorphous fractions of polylactide. *Macromolecules* **2014**, *47*, 5186–5197.
55 Zhang, J.; Duan, Y.; Sato, H.; Tsuji, H.; Noda, I.; Yan, S.; Ozaki, Y. Crystal modifications and thermal behavior of poly(L-lactic acid) revealed by infrared spectroscopy. *Macromolecules* **2005**, *38*, 8012–8021.
56 Zhang, T.; Hu, J.; Duan, Y.; Pi, F.; Zhang, J. Physical aging enhanced mesomorphic structure in melt-quenched poly(L-lactic acid). *J. Phys. Chem. B* **2011**, *115*, 13835–41.
57 Kister, G.; Cassanas, G.; Vert, M.; Pauvert, B.; Térol, A. Vibrational analysis of poly(L-lactic acid). *J. Raman Spectrosc.* **1995**, *26*, 307–311.
58 Liang, Y. Y.; Tang, H.; Zhong, G. J.; Li, Z. M. Formation of poly(L-lactide) mesophase and its chain mobility dependent kinetics. *Chinese J. Polym. Sci* **2014**, *32*, 1176–1187.
59 Hu, J.; Han, L. L.; Zhang, T. P.; Duan, Y. X.; Zhang, J. M. Study on phase transformation behavior of strain-induced PLLA mesophase by polarized infrared spectroscopy. *Chinese J. Polym. Sci.* **2019**, *37*, 253–257.
60 Li, Y. P.; Xin, R.; Wang, S. J.; Guo, Z. X.; Sun, X. L.; Ren, Z. J.; Li, H. H.; Li, L.; Yan, S. K. Structure and mechanical property of melt-drawn oriented PLA ultrathin films. *Macromolecules* **2021**, *54*, 9124–9134.

https://doi.org/10.1007/s10118-022-2723-3